Desalination and Water Treatment
www.deswater.com

doi: 10.5004/dwt.2023.29576

294 (2023) 162–171
May

Highly efficient adsorption of U(VI) from aqueous solution by the terpolymer of acrylonitrile/acrylic acid-*co*-hydroxyapatite

Ruixia Wang[a,†], Huining Tian[a,†], Xiaolan Jin[b], Yifu Zhang[a], Tonghuan Liu[c,d], Guojian Duan[a,*], Hui Chen[a,*]

[a]*Northwest Collaborative Innovation Center for Traditional Chinese Medicine Co-Constructed by Gansu Province & MOE of PRC, College of Pharmacy, Gansu University of Chinese Medicine, Lanzhou 730000, China, emails: duangj@gszy.edu.cn (G.J. Duan), chenh@gszy.edu.cn (H. Chen), 2979963116@qq.com (R.X. Wang), tian05082018@126.com (H.N. Tian), 229383664@qq.com (Y.F. Zhang)*
[b]*First School of Clinical Medical, Gansu University of Chinese Medicine, Lanzhou 730000, China, email: 1283250266@qq.com (X.L. Jin)*
[c]*Radiochemistry Laboratory, School of Nuclear Science and Technology, Lanzhou University, Lanzhou 730000, China, email: liuth@lzu.edu.cn (T.H. Liu)*
[d]*Key Laboratory of Special Function Material and Structure Design Dinistry Education, School of Nuclear Science and Technology, Lanzhou University, Lanzhou 730000, China*

Received 24 November 2022; Accepted 18 April 2023

ABSTRACT

To better eliminate the impact of radioactive elements on the environment, we synthesized a terpolymer of acrylonitrile, acrylic acid, and hydroxyapatite (AN/AA-*co*-HAP) as an adsorption material for separating uranyl ions in aqueous solution, which was based on our previous work. We used Fourier-transform infrared spectroscopy, scanning electron microscopy, elemental analysis, N_2 sorption/desorption isotherm, thermogravimetric analysis and X-ray diffraction methods to characterize the material's structure, and studied the effect of equilibrium time, pH, ionic strength, solid–liquid ratio, initial concentration, and temperature on the adsorption process. Finally, it is concluded that adsorption equilibrium can be reached within 60 min at room temperature, and the maximum adsorption capacity is 343.3 mg/g. Thermodynamic analysis indicates that the adsorption process is a spontaneous endothermic process. In the system with a nitric acid concentration of 0.05 mol/L (pH value: 1.3), the desorption rate of U(VI) can reach 91%, while the adsorption rate of U(VI) in aqueous solution onto AN/AA-*co*-HAP is still remains >60% even after the material is has been reused 6 times. These results suggest that AN/AA-*co*-HAP is highly valuable for treating U(VI) ions in aqueous solution.

Keywords: Adsorption; Terpolymer; Hydroxyapatite; Acrylonitrile; Acrylic acid; U(VI)

1. Introduction

Nuclear energy has been widely used in military, energy and other fields for its high efficiency and low carbon characteristics [1]. However, the use of nuclear energy, mismanagement of nuclear waste, and nuclear leakage, etc., can inevitably result in radioactive contamination. Once radionuclides enter water, will they not only pose a threat to aquatic organisms and the ecological environment but may also enter human body through the food chain. Due to their radioactivity, chemical toxicity, and biological accumulation, can lead to leukaemia, cancer, and even death

* Corresponding authors.
† These authors contributed equally to this work.

[2–4]. For instance, the "World Health Organization" and the United States have set the maximum amount of uranium ions in drinking water at 30 μg/L [5]. Nuclear waste contains various radioactive elements (uranium, strontium, caesium, plutonium, etc.), of which uranium(VI) is the main component, so here is an urgent need for the safe and effective removal of uranium ions from wastewater.

Various methods have been developed to remove uranium from contaminated water, but the adsorption method has widely gained attention due to its low cost, environmentally eco-friendliness, and high efficiency [6–9]. The development of new adsorbents has become the key issue in this field. Carbon fiber [10,11] carbon nanotubes [12,13], graphene oxide [14], MOFs [1] and COFs [15] materials have been as potential sorbents investigated for removing U(VI) from contaminated groundwater. Nonetheless, many of these novel adsorbent materials have drawbacks such as high cost, low adsorption capacity or low removal rate, which limit their practical application.

Generally, a good adsorption material should have favorable properties such as a stable porous structure and functional groups that combine easily with heavy metal ions, as well as being rich in natural content. Hydroxyapatite (HAP), a natural mineral containing phosphate, has been widely used in medicine due to its similarity in composition to human bone and a Ca/P molar ratio of 1.67 [16–18]. Additionally, its high porosity, good buffering performance, low water solubility, the presence of Ca^{2+}, OH^-, and PO_4^{3-} groups in its structure allow for the electrostatic interaction or ion exchange with a range of metal ions such as Cd^{2+}, Zn^{2+}, Pb^{2+}, Co^{2+}, UO_2^{2+}, etc. [19–25]. Therefore, HAP materials are also commonly used in treating wastewater containing heavy metal ions. Since HAP is a white powder and difficult to separate from the water phase, modified hydroxyapatite can improve both its solid–liquid separation performance and its adsorption capacity for specific metal ions. For example, Liu et al. [26] reported that BioHAP is a suitable material for the remediation of metal-contaminated water bodies and the storage of radionuclide waste, respectively, with a reported maximum adsorption capacity of 755 mg/g. Han et al. [27] synthesized Bio-HAP600 with S_{BET} of 74.4 m^2/g from fresh bones by calcination, which could achieve adsorption equilibrium within 10 min, and the maximum adsorption capacity was 384.6 mg/g at pH of 3.0; Wu et al. [28] found that the preparation of layered hollow hydroxyapatite microspheres could be developed as excellent adsorbents for the removal of U(VI) ions, with a maximum adsorption capacity of 199 mg/g. El-Maghrabi et al. [29] proposed a simple microwave-assisted synthesis of magnetically modified hydroxyapatite nanoparticles, with adsorption equilibrium reached within 120 min, and the maximum adsorption capacity of uranium is 310 mg/g.

Prior to this study, our group has reported on the use of polyacrylic acid-hydroxyapatite composite material [30] and hydroxyapatite composite material with amine oxime faculties [31] in the adsorption of U(VI) ions in aqueous solution. In order to gain a better understanding of the adsorption performance of this type of material, this paper presents the synthesis and structural characterization of the terpolymer of acrylonitrile, acrylic acid, and hydroxyapatite (AN/AA-*co*-HAP), and studies the thermodynamics and kinetics of the U(VI) separation process. The optimal adsorption conditions were determined by examining various influencing factors, such as pH value, solid–liquid ratio, initial U(VI) concentration and ionic strength of the solution. As a continuation of our research on the adsorption behavior of functional hydroxyapatite composites for uranyl ions, this paper provides experimental support for a comprehensive understanding of this kind of adsorption materials and the optimization of their adsorption conditions.

2. Materials and methods

2.1. Materials

The chemicals used in the experiment were as follows: calcium hydroxide (98%, Sinopharm Chemical Reagent Co., Ltd., China); phosphoric acid (85 wt.%, Xiyashiji Company, Linyi, China); *N*,*N*′-Methylenebisacrylamide (>99%, Sinopharm Chemical Reagent Co., Ltd., Shanghai, China); potassium persulfate (99.5%, J&K Scientific, Beijing, China); acrylonitrile (AN, >99%, Xiyashiji Company, Chengdu, China); acrylic acid (AA, 99%, Anhui Senrise Technology Co., Ltd., Shanghai, China); uranyl nitrate hexahydrate (99%, Beijing Wokai Biotechnology Co., Ltd., Beijing, China); arsenazo III (>95%, Anhui Senrise Technology Co., Ltd., Shanghai, China). All the other chemicals were of analytical grade and deionized water was used unless stated otherwise.

Uranyl nitrate stock solution was prepared by dissolving uranyl nitrate hexahydrate ($UO_2(NO_3)_2{\cdot}6H_2O$) in deionized water. The pH of the working solution was adjusted to the desired value by the addition of 0.5 M HNO_3 or 0.5 M NaOH aqueous solutions.

2.2. Characterization

The contents of C, H, N were measured by an elemental analyzer (Vario EL, Elementar, Hanau, Germany), which were used to estimate the proportions of each monomer in the copolymer. The morphological features of three proportional copolymers were examined by the scanning electron microscopy (SEM, Hitachi S-4800, Tokyo, Japan). A Fourier-transform infrared spectroscopy (FTIR) spectrum spectrometer (Nicolet Avatar 360, Thermo Nicolet, Waltham, MA, USA) was used to characterize the material functional group identifications in the range between 4,000~500 cm^{-1} by mixing 0.01 g of the material with 0.1 g KBr (spectroscopy grade) pellets. The specific surface area and pore size were characterized by N_2 adsorption/desorption isotherm experiments (Micromeritics, ASAP 2020 V4.01, Georgia, USA). The thermal stability was conducted by a thermogravimetric analyzer (STA PT 1600, LINSEIS, Germany). X-ray diffractometer (XRD, Shimadzu XD-l) was used to indicate the phases exist in the material.

2.3. Preparation of AN/AA-co-HAP composite

AN/AA-*co*-HAP composite was synthesized by the following procedures previously reported in our research [31]. Under N_2 protection and at 55°C, H_3PO_4 (0.3 M, 25 mL) was added dropwise to $Ca(OH)_2$ aqueous solution (0.25 M, 50 mL), and after stirring for 30 min, equal molar amounts of

acrylonitrile and acrylic acid were added to the reaction system at the same time to make HAP:AN:AA = 1:1:1~1:10:10. Subsequently, cross-linking agent (*N*,*N*′-methylene acrylamide) and initiator (potassium persulfate) were added, the reaction temperature was raised to 65°C, and the reaction was then allowed to proceed overnight under agitation. After completion of the reaction, the generated precipitate was separated by centrifugation and washed 5 times with deionized water to remove unreacted reagents, followed by drying in a vacuum chamber. The product was ground and sieved down to 200 mesh size. The samples were characterized by means of attenuated total FTIR and SEM.

2.4. Batch adsorption experiments

To conduct the adsorption experiments, a predetermined amount of adsorbent was added to a fixed concentration of U(VI) stock solution, and the pH of the reaction system was adjusted to the desired value by a 0.5 M sodium hydroxide aqueous solution, where the volume of solution was kept at 5.00 mL using deionized water. The reaction system was then stirred for 6 h at 25°C. The concentration of U(VI) was analyzed using a Shimadzu UV-723N spectrophotometer: specifically, 1.00 mL of the U(VI) supernatant after reaching adsorption equilibrium was mixed with 1.00 mL of 0.5 M HCl, 2.00 mL of 1 g/L arsenazo III solution, and 21.00 mL deionized water were added to in a 25 mL volumetric flask. After 20 min, the absorbance of the mixture was measured at 652 nm [30], and the concentration of U(VI) ions for the filtrate was calculated by comparing it with the standard curve of the uranium solution.

The effects of various factors on the adsorption performance were evaluated by varying the equilibrium time, ionic strength, initial adsorbent dose, pH value, and U(VI) concentration. The percentage adsorption on the adsorbent (adsorption ratio%) and the amounts of adsorbed ions q_e (mg/g) were calculated according to the following equations:

$$\text{Adsorption ratio\%} = \left[\frac{\left(C_0 - C_e\right)}{C_0}\right] \times 100\% \quad (1)$$

$$q_e = \left[\frac{\left(C_0 - C_e\right)}{m}\right] \times V \quad (2)$$

where C_0 (mg/L) and C_e (mg/L) are the U(VI) concentrations of the liquid phase at initial time and equilibrium time, respectively; V is the volume of the solution (L); m is the weight of dry adsorbent used (g).

2.5. Desorption and reuse

The adsorbent bound to uranyl ion was obtained by centrifugation and dried in a vacuum oven at 60°C for 2 d. The adsorbent was then placed in a nitric acid solution (5.00 mL) of different concentrations, and stirred at room temperature for 2 h, the desorption rate under this condition can be determined by measuring the concentration of U(VI) in the solution, which can be calculated by Eq. (3):

$$\text{Desorption rate}(\%) = \left[\frac{C_{dN}}{\left(C_{0N} - C_{eN}\right)}\right] \times 100\% \quad (3)$$

where C_{0N} (mg/L), C_{eN} (mg/L) and C_{dN} (mg/L) represent the U(VI) concentrations of the liquid phase supernatant at the initial time and the equilibrium time of the *N*th sorption/desorption cycle, and after desorption by HNO_3, respectively.

3. Results and discussion

3.1. Characterization

3.1.1. Elemental analysis

Table 1 displays the results of the elemental analysis results of AN/AA-*co*-HAP synthesized with different ratios. The molar ratio of AN in the terpolymer can be calculated based on the mass percentage of N, and the molar ratio of AA can be computed based on the mass percentage of C, with the remainder being HAP. Therefore, the actual ratio of the three monomers in the composite was determined. The results also indicate that the content of HAP in the actual terpolymer is lower than the theoretical amount, possibly due to the incomplete reaction of calcium hydroxide and phosphoric acid, leading to the formation of less HAP than anticipated. The results obtained from the three different proportions are consistent.

3.1.2. Scanning electron microscopy

The morphologies of AN/AA-*co*-HAP with different proportions were characterized by SEM, and the results are shown in Fig. 1a–c.

From the SEM results, it can be observed that the microstructure of this kind of material changes with variations in its composition ratio. When the HAP content is high (material 1), the structure is relatively compact and the pore size of the particle surface is small. Material 3 exhibits obvious surface characteristics of high polymer, and it even tends to encapsulate hydroxyapatite inside. In order to better reflect the stable structural support of hydroxyapatite

Table 1
Elemental analysis of AN/AA-*co*-HAPs

	Theoretical value of	N%	C%	H%	Practical value of
	HAP:AN:AA (molar ratio)				HAP:AN:AA (molar ratio)
Material 1	1.00:1.00:1.00	1.582	9.334	1.126	1.00:1.36:1.76
Material 2	1.00:3.00:3.00	3.075	17.765	1.951	1.00:3.21:4.01
Material 3	1.00:10.00:10.00	6.645	36.865	3.704	1.00:13.51:15.64

and the adsorption ability of its surface-active functional groups, the loose network structure characteristics formed by the polymerization of its unsaturated organic molecules, and the coordination ability of its coordination functional groups for metal ions, the AN/AA-*co*-HAP of material 2 was used as the adsorbent material in this study, and its adsorption performance has been also evaluated accordingly. This decision is consistent with the results of preliminary experiments. As can be seen from Fig. 1d–e, the material is loose and porous before binding with uranyl ions, but after binding with uranyl ions, the porous structure on the surface of the material disappears, showing a compact and smooth state (Fig. 1f–g), all this indicating that the adsorption process has reached equilibrium.

3.1.3. Fourier-transform infrared spectroscopy

As shown in Fig. 2, the stretching vibration peak (2,246.9 cm^{-1}) of the cyano group (−C≡N) indicates that acrylonitrile molecules have been successfully introduced into the composite [32]. The absorption peak at 1,034.7 cm^{-1} is attributed to the stretching vibration peak of P=O, while the symmetric stretching vibration absorption is observed at 962.32 cm^{-1}, and the bending vibration absorption is observed at 563.4 and 603.3 cm^{-1} for the P–O bond. All of these indicate that the PO_4^{3-} group is present in the composite structure [33,34]. Moreover, the stretching vibration absorption peak of the C=O bond at 1,724.4 cm^{-1} and the stretching vibration absorption peak of −OH at 2,938.6 cm^{-1} prove the existence of acrylic structural units in the composite [32,35].

3.1.4. Specific surface area

The Brunauer–Emmett–Teller (BET) measurements were investigated using nitrogen sorption and desorption method as displayed in Fig. 3a. The nitrogen sorption/desorption isotherm of AN/AA-*co*-HAP and AN/AA-*co*-HAP-UO_2^{2+} are the type III curve of for a microporous material, and the calculated specific surface area is 71.29 m^2/g and the average pore diameter is 32.50 nm. When combined with uranyl ion, the specific surface area of the AN/AA-*co*-HAP becomes to 27.55 m^2/g and the average pore diameter is reduced to 12.38 nm. These results are consistent with SEM results.

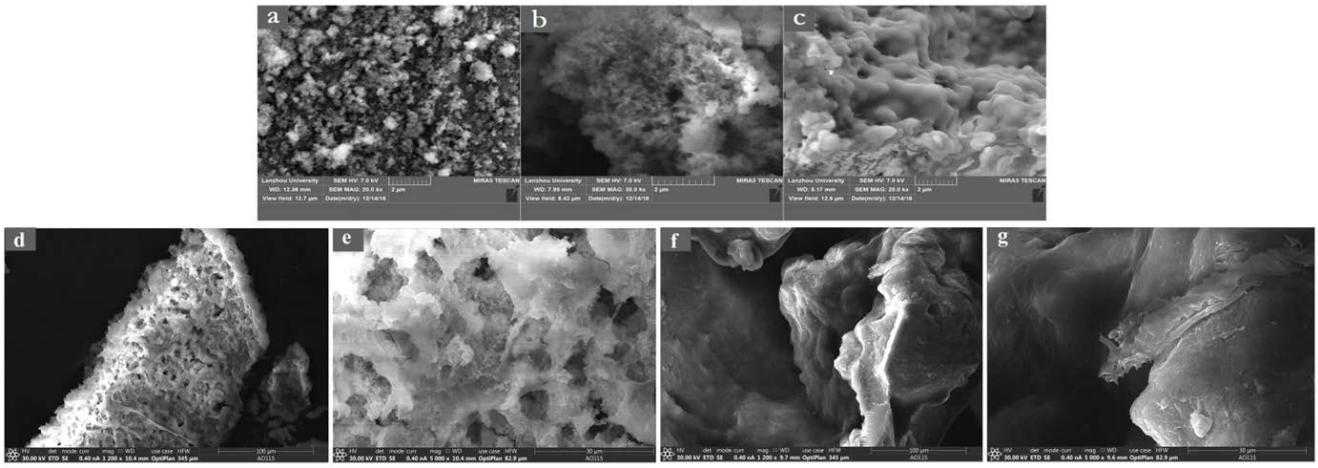

Fig. 1. Scanning electron microscopy of AN/AA-*co*-HAPs. (a) Material 1, (b) material 2, (c) material 3, (d) AN/AA-*co*-HAP (100 μm), (e) AN/AA-*co*-HAP (30 μm), (f) AN/AA-*co*-HAP-UO_2^{2+} (100 μm) and (g) AN/AA-*co*-HAP-UO_2^{2+} (30 μm).

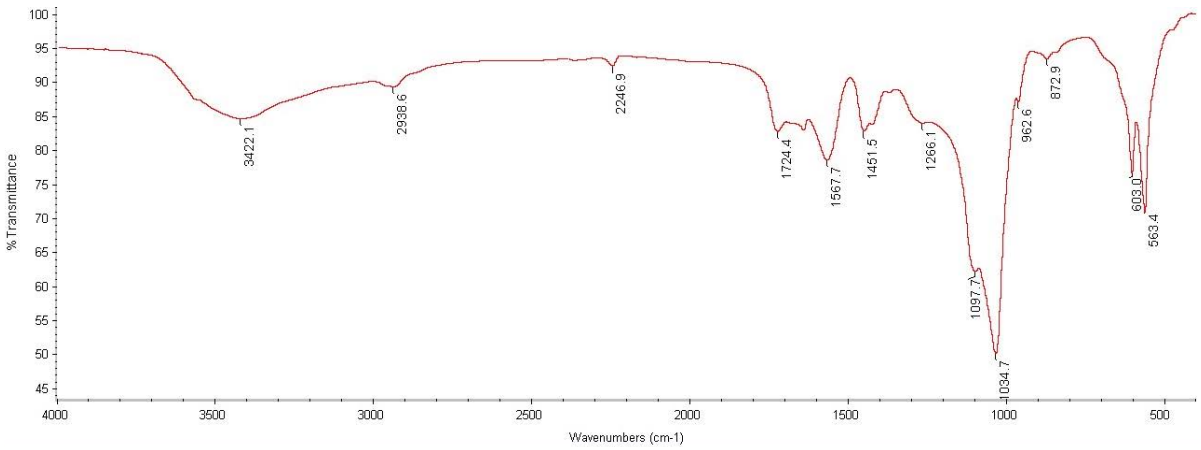

Fig. 2. Fourier-transform infrared spectrum of AN/AA-*co*-HAP (material 2).

3.1.5. Thermogravimetric analysis

The thermal stability of AN/AA-*co*-HAP was analyzed by thermogravimetric analysis (TGA). The results, depicted in Fig. 3b, reveal that there are two distinct weight loss processes occurring at 70°C–160°C and 320°C–530°C. The first mass loss process can be attributed to the volatilization of water and other solvents in the material, while the second process can be regarded as the decomposition of AN/AA-*co*-HAP chain. Overall, AN/AA-*co*-HAP exhibits good thermal stability.

3.1.6. X-ray powder diffraction analysis

X-ray diffraction (XRD) can investigate the phase structure and the crystallinity extent of the material. The XRD patterns of AN/AA-*co*-HAP and AN/AA-*co*-HAP-UO_2^{2+} are shown in Fig. 3c. It can be seen from the results that, due to the introduction of copolymer, the crystallinity of the adsorbed material is significantly lower than that of HAP, but the diffraction peaks near 34° indicated that the crystal structure of HAP is still preserved in the AN/AA-*co*-HAP. At the same time, there is no obvious difference between the XRD patterns of AN/AA-*co*-HAP and AN/AA-*co*-HAP-UO_2^{2+}, indicating that the introduction of uranyl ions does not affect the structure of the adsorbed materials.

3.2. Adsorption performance study

3.2.1. Adsorption kinetics

Adsorption kinetics studies allow for predicting the adsorption rate of adsorbents, which is crucial in evaluating the practical application potential of this type of adsorbent. Fig. 4 depicts the relationship between the adsorption capacity of AN/AA-*co*-HAP with three different proportions for U(VI) ions and their contact time. The results demonstrate that the adsorption process can be divided into two stages: in the first stage, the adsorption equilibrium has not been reached, there are many empty binding sites on the surface of the AN/AA-*co*-HAP, leading to a rapid increase in the adsorption capacity. Within 30–60 min, the adsorption rate of uranyl ions and desorption rate of AN/AA-*co*-HAP tend to be consistent, and the adsorption amount is close to the maximum. In the second stage, the adsorption reaction maintains dynamic equilibrium, and the adsorption capacity and the adsorption rate will not increase significantly with the extension time.

At the same time, it can also be seen that the first adsorption stage of material 1 is similar to that of material 2, but its maximum adsorption capacity is lower than material 2. The adsorption rate and maximum adsorption capacity of material 3 are also lower than those of material 2. Combining these findings with the SEM results, it can be inferred that the surface of material 1 has an obvious granular nature, which facilitates the rapid binding of uranyl ions to the adsorbent during the first stage of the adsorption process. However, the relative surface area of material 1 is smaller than that of material 2, resulting in a lower maximum adsorption capacity. Material 3 exhibits clear polymer properties, which leads to a slower increase in its adsorption rate during the first stage. Owing to the higher content of cyanide and carboxyl groups in material 3, its maximum adsorption capacity falls between those of materials 1 and 2.

The kinetic study of this adsorption reaction is very important to understand the physical and chemical changes of this process. In this paper, typical adsorption kinetic

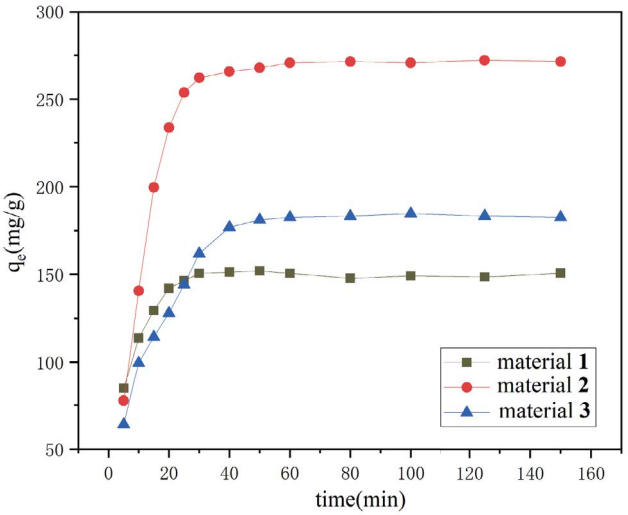

Fig. 4. Relationships between the adsorption capacity of materials 1, 2 and 3 for U(VI) ions and contact time. (C_0[U(VI)] = 8.2 × 10^{-5} mol/L; solid/liquid ratio = 0.03 g/L; pH = 3.00 ± 0.05; T = 298.15 ± 1.00 K).

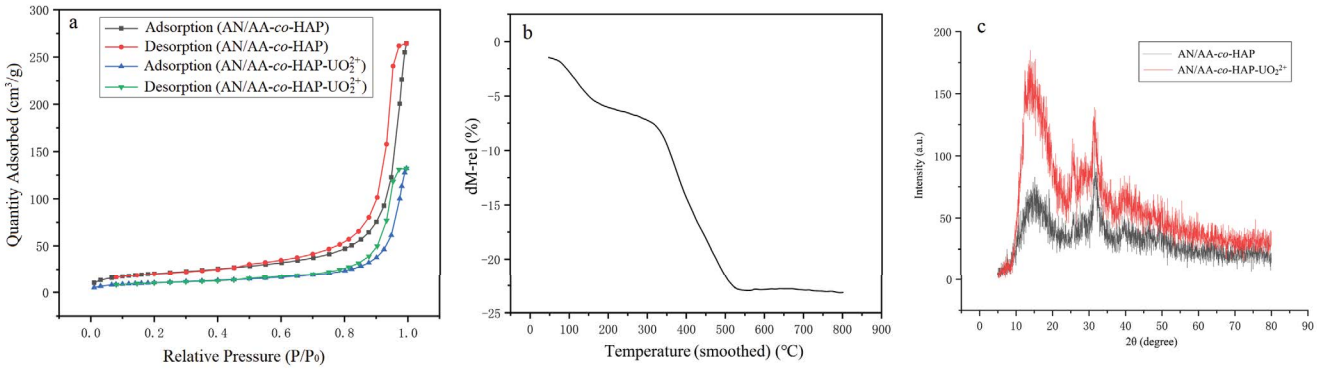

Fig. 3. N_2 sorption/desorption isotherm (a), thermogravimetric analysis (b) and the X-ray diffraction patterns (c).

models are used to fit adsorption data: pseudo-first-order and pseudo-second-order models, and their linear mathematical expressions, are shown in Eqs. (4) and (5), respectively:

$$\ln\left(q_{e1}-q_t\right)=\ln q_{e1}-K_1 t \tag{4}$$

$$\frac{t}{q_t}=\frac{1}{\left(K_2 q_{e2}^2\right)}+\frac{t}{q_{e2}} \tag{5}$$

where K_1 (min^{-1}) and K_2 (g/mg·min) are the rate constants of the two models, respectively. q_{e1} (mg/g) and q_{e2} (mg/g) are the calculated equilibrium adsorption capacities of metal ions, while q_t (mg/g) is the adsorption capacity of metal ion at time t.

Table 2 shows the results of the kinetic parameters indicating that the coefficient of determination (R^2) of the pseudo-second-order kinetics model is 0.9952, which is closer to 1 than pseudo-first-order kinetics model. Meanwhile, the equilibrium adsorption quantity derived by the pseudo-second-order linear mathematical expression is more consistent with the experimental data. Therefore, the proposed secondary dynamics model is better suited to describe the adsorption reaction process, and the adsorption rate is more dependent on the availability of active adsorbent sites than the concentration of metal ions. The bonding between uranyl ions and the adsorbents involves a valence force through the sharing or exchanging of electrons, which is classified as a chemical adsorption process [36,37].

3.2.2. Effect of pH value and ionic strength

The pH value of radioactive waste liquid plays a critical role in determining the predominant form of U(VI) ions and the surface chemistry of AN/AA-*co*-HAP. Therefore, it is one of the most important factors to investigate the potential of adsorbent materials for practical applications.

The stability of the terpolymer decreases under strong acid conditions, which reduces the number of times it can be reused. As the pH value increases, uranyl ions undergo a hydrolysis reaction. When the pH value is above 4.5, the proportion of free uranyl ions decreases significantly, while the proportion of hydroxide forms of uranyl ions (UO_2OH^+, $(UO_2)_2(OH)_2^{2+}$, $(UO_2)_3(OH)_5^+$, etc.) increases. To better study the adsorption behavior of AN/AA-*co*-HAP on uranyl ions, in this section, the pH value of the solution is controlled between 2.0~5.5.

Table 2
Kinetic parameters for U(VI) adsorbed onto AN/AA-*co*-HAP

Kinetic model	Model parameters	Results
Pseudo-first-order kinetic model	K_1 (min^{-1})	5.85×10^{-2}
	q_{e1} (mg/g)	17.09
	R^2	0.8513
Pseudo-second-order kinetic model	K_2 (g/mg·min)	5.75×10^{-4}
	q_{e2} (mg/g)	285.71
	R^2	0.9952

It can be seen from Fig. 5 that the adsorbance increases with the increasing of the solution pH value. According to the literature [38], there is no significant change in the adsorption performance of hydroxyapatite to uranyl ions in the range of pH 3–8, thus the change observed in this experiment should be due to the changes of carboxylic acid groups and uranyl ions.

Since acrylic acid remains an organic acid after polymerization, and its pKa value is around 4–5, ion exchange reactions between uranyl ions and carboxylic acid groups are hindered under the condition of strong acidity. However, the increased U(VI) adsorption at pH 4.0–5.5 could be ascribed to the tendency of carboxylic acid groups to exist in the form of carboxylate ions, which enhanced their binding ability with uranyl ions. Additionally, the repulsion between like charges increases the swelling capacity, promoting the combination of uranyl ions with the active sites of the adsorbent material; and the surface co-precipitation of the U(VI) (i.e., schoepite) may also occur [39].

In order to study the binding mechanism between AN/AA-*co*-HAP and uranyl ions, all subsequent experiments were conducted at a pH value of 4.0 ± 0.1. When a NaCl solution was added to alter the ionic strength of the solution, the results (Fig. 4) demonstrated that the adsorption properties of this kind of adsorbent remained almost unchanged, indicating that inner-sphere surface complexation dominated U(VI) sorption on AN/AA-*co*-HAP [39].

3.2.3. Effect of solid/liquid ratio

Fig. 6 shows the relationship among solid/liquid ratio, adsorption capacity, and adsorption rate. With an increase in the solid/liquid ratio, the adsorption rate increases, but the adsorption capacity gradually decreases. This is because, at the initial stage, the low content of the adsorbent in the solution results in an insufficient number of sites available to bind with U(VI) ions, which leads to a high level of adsorption capacity. As the solid/liquid ratio increases, the concentration

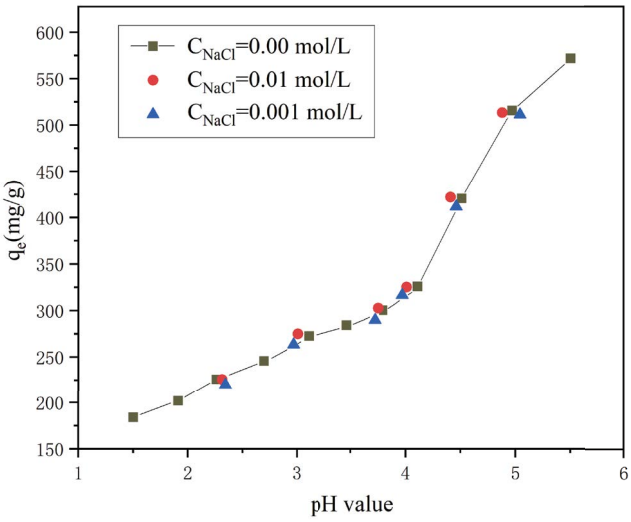

Fig. 5. Effect of pH value and ionic strength. (C_0[U(VI)] = 8.2 × 10^{-5} mol/L; solid/liquid ratio = 0.03 g/L; T = 298.15 ± 1.00 K; t = 2.0 h).

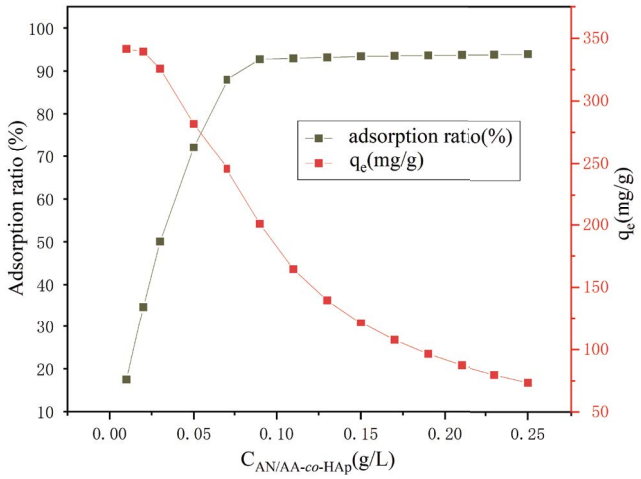

Fig. 6. Effect of solid/liquid ratio (C_0[U(VI)] = 8.2 × 10^{-5} mol/L; pH = 4.00 ± 0.05; T = 298.15 ± 1.00 K; t = 2.0 h).

of U(VI) ions in the solution drops significantly, leading to a decrease in adsorption capacity. Once a dynamic equilibrium is established between the adsorbed and free U(VI) ions, the adsorption rate remains relatively stable. When the solid/liquid ratio is 0.09 g/L, the adsorption rate is 92.7%, indicating that AN/AA-*co*-HAP exhibits good adsorption performance for U(VI).

3.2.4. Effect of the initial concentration of U(VI) and adsorption thermodynamics

Fig. 7 shows the effect of the initial concentration of U(VI) ions on the adsorption capacity of AN/AA-*co*-HAP at different temperatures (298.15, 318.15 and 338.15 K). The results suggest that increasing the temperature is conducive to the adsorption of U(VI) ions onto AN/AA-*co*-HAP. In addition, the adsorption capacity increases with the initial concentration, and can reach a maximum value.

In order to understand the surface properties and adsorption mechanism of the adsorbent, Langmuir and Freundlich adsorption isotherm models were used to simulate the adsorption process [40]. The linear form of Langmuir equation is shown as Eq. (6):

$$\frac{C_e}{q_e} = \frac{1}{\left(K_L \cdot q_{\max}\right)} + \frac{C_e}{q_{\max}} \tag{6}$$

where C_e is the equilibrium concentration of U(VI) in solution (mg/L), q_e is the adsorption capacity at adsorption equilibrium (mg/g), $q_{\max}$ is the maximum adsorption capacity (mg/g), K_L is the adsorption equilibrium constant (L/mg). The assumptions of the Langmuir isothermal model are as follows: monolayer surface adsorption, the adsorption sites are the same, and the adsorbed particles are completely independent. The adsorption capacity increased with the increase in temperature under the same conditions, indicating that the adsorption process was endothermic, and the interaction between U(VI) and the active site of AN/AA-*co*-HAP could be promoted with the increase of temperature.

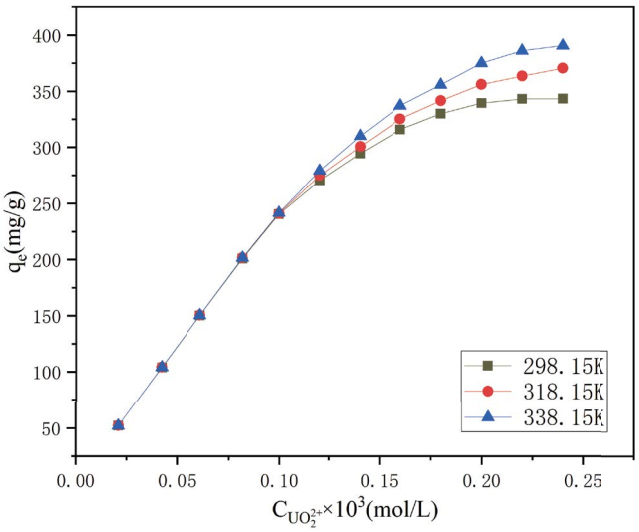

Fig. 7. Effect of the initial concentration of U(VI) and the temperature of the solution to adsorption process. (C_0[U(VI)] = 2.1 × 10^{-5} ~ 2.4 × 10^{-4} mol/L; solid/liquid ratio = 0.09 g/L; pH = 4.00 ± 0.05; t = 2.0 h).

Table 3
Constants of Langmuir and Freundlich model

	T (K)	K_L (L/g)	$q_{\max}$ (mg/g)	R^2
Langmuir model	298.15	0.675	370.4	0.9995
	318.15	0.595	400.0	0.9993
	338.15	0.558	416.7	0.9993
	T (K)	K_F (mg^{1-n}/L^n·g)	n	R^2
Freundlich model	298.15	135.46	2.75	0.8461
	318.15	137.84	2.60	0.8668
	338.15	139.05	2.41	0.8811

The Freundlich isotherm model is an empirical equation with no assumptions [41], and its linearization form is shown as Eq. (7):

$$\ln q_e = \ln K_F + \frac{1}{n}\ln C_e \tag{7}$$

where K_F (mg^{1-n}/L^n·g) and n are characteristic constants related to the relative adsorption capacity and adsorption strength, respectively.

The experimental results show that the Langmuir isotherm model is more suitable to describe the adsorption process than the Freundlich isotherm model, and the predicted maximum adsorption capacity matches the experimental value. The relevant fitting results are shown in Table 3.

Based on the above experimental results, the van't Hoff equation can be used to calculate the changes of thermodynamic parameters in the adsorption process, which helps us to analyze the adsorption process.

$$\ln K_L = \frac{\Delta S^\circ}{R} - \frac{\Delta H^\circ}{RT} \tag{8}$$

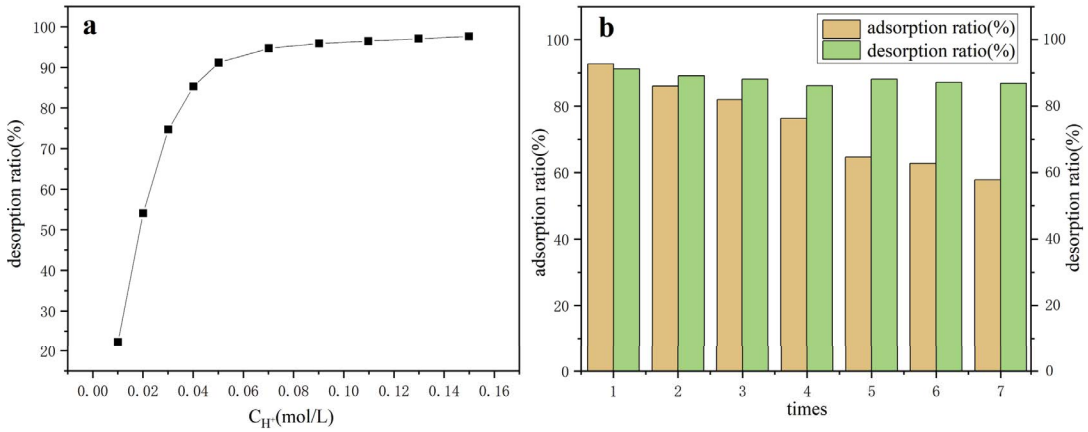

Fig. 8. Desorption and reuse capacity of AN/AA-*co*-HAP (C_0[U(VI)] = 8.2 × 10^{-5} mol/L; solid/liquid ratio = 0.09 g/L; $pH_{adsorption}$ = 4.00 ± 0.05; $[H^+]_{desorption}$ = 0.05 mol/L; T = 298.15 ± 1.00 K; t = 2.0 h).

Table 4
Thermodynamic parameters

T (K)	$\Delta G°$ (kJ/mol)	$\Delta H°$ (kJ/mol)	$\Delta S°$ (J/mol·K)
298.15	–35.60		
318.15	–38.10	1.56	124.65
338.15	–40.59		

Table 5
Values of separation factor (SF) for $(UO_2)^{2+}$ vs. five metal ions

	$(UO_2)^{2+}$/ Mg^{2+}	$(UO_2)^{2+}$/ Cu^{2+}	$(UO_2)^{2+}$/ Zn^{2+}	$(UO_2)^{2+}$/ Ni^{2+}	$(UO_2)^{2+}$/ Pb^{2+}
SF	29.56	19.22	15.21	25.49	16.63

$$\Delta G° = \Delta H° - T\Delta S° \quad (9)$$

where R is the universal gas constant (8.314 J/mol·K) and T is the thermodynamic temperature (K). The detailed values of $\Delta G°$, $\Delta H°$ and $\Delta S°$ are listed in Table 4.

As can be seen from Table 4, $\Delta G°$ values are all negative, indicating that the binding process between the adsorbent and U(VI) ions is spontaneous. $\Delta G°$ decreases with the increase of temperature, which indicates that the adsorption process is endothermic. The affinity of AN/AA-*co*-HAP increases with the increase of temperature [42], which is consistent with the experimental results that the adsorption capacity (343.3 ~ 370.5 ~ 390.6 mg/g) increases with the increase of temperature (298.15 ~ 318.15 ~ 338.15 K).

3.2.5. Desorption and reuse

The desorption capacity and reusability of an adsorbent determine its potential for practical application. Based on previous practical experience, we conducted experiments on the reaction system for uranyl ion desorption with different concentrations of nitric acid solution. Fig. 8a shows that the desorption rate of uranyl ions is related to the acid strength of the system. At a concentration of 0.05 M nitric acid (pH value is 1.3), the desorption rate was greater than 91%. This result suggests that the uranyl ions were bonded to the adsorbent through ion exchange that forms ionic bonds or coordination bonds [36].

As shown in Fig. 8b, the experimental results of adsorption and regeneration indicated that AN/AA-*co*-HAP can effectively repeat 6 cycles of the adsorption/desorption process (adsorption ratio >60%), which indicates that this adsorbent has good application potential for the enrichment of uranyl ions in aqueous solution.

3.2.6. Selective adsorption of uranyl ions

Since a variety of ions coexist with uranyl waste liquid systems, so it is necessary to determine the interactions between ions and the influence on the adsorption capacity of materials during the adsorption process. In this experiment, Mg^{2+}, Cu^{2+}, Zn^{2+}, Ni^{2+} and Pb^{2+} were selected as coexisting competitive ions, and the concentration of each ion was set at 8.0 × 10^{-5} mol/L. The concentration of metal ions was determined by atomic absorption spectrometry (AAnalyst 700, PerkinElmer Company, Waltham, MA, USA).

It can be seen from the results of the separation factor values (as shown in Table 5) that the adsorption capacity of AN on U(VI) is significantly higher than that of other coexisting ions. Furthermore, it can also be inferred that the existence of coexisting ions has no obvious influence on the adsorption process.

4. Conclusions

In this paper, AN/AA-*co*-HAP was used as an adsorbent to remove uranyl ions from the radioactive waste liquid. According to the kinetic study, the adsorption process can be well described by the pseudo-second-order model. Therefore, we inferred that U(VI) ions and AN/AA-*co*-HAP combined through valence forces by sharing or exchanging electrons, which belongs to the chemical adsorption process. The Langmuir isothermal model showed that uranyl ions combined with the adsorbent as a monolayer surface form, and there was no interaction between metal ions.

The thermodynamic study of the adsorption process showed that the binding of uranyl ions with adsorbent materials was a spontaneous endothermic process. The above results provide experimental data to support the further development of such adsorbents.

Funding

This research was funded by:

- "In 2022, Gansu Province Higher Education Youth Doctor Foundation Project, Grant Number 2022QB-098";
- "Science and Technology Project of Gansu Province, Grant Number 21JR1RA265";
- "Gansu University of Chinese Medicine Postgraduate Innovation Fund, Grant Number 2021CX43";
- "Key Scientific Research Projects of Gansu Institute of Traditional Chinese Medicine, Grant Number 2305137402".

References

[1] B. Zhao, L.Y. Yuan, Y. Wang, T. Duan, W.Q. Shi, Carboxylated UiO-66 tailored for U(VI) and Eu(III) trapping: from batch adsorption to dynamic column separation, ACS Appl. Mater. Interfaces, 13 (2021) 16300−16308.
[2] K.R. Zhu, G. Song, X.M. Ren, C.L. Chen, Solvent-free engineering of Fe^0/Fe_3C nanoparticles encased in nitrogen-doped carbon nanoshell materials for highly efficient removal of uranyl ions from acidic solution, J. Colloid Interface Sci., 575 (2020) 16–23.
[3] B.L. Wang, Y.Y. Li, J.L. Zheng, Y.W. Hu, X.J. Wang, B.W. Hu, Efficient removal of U(VI) from aqueous solutions using the magnetic biochar derived from the biomass of a bloom-forming cyanobacterium (*Microcystis aeruginosa*), Chemosphere, 254 (2020) 126898, doi: 10.1016/j.chemosphere.2020.126898.
[4] C. Jiang, Y. Liu, D.Z. Yuan, Y. Wang, J.B. Liu, J.W. Chew, Investigation of the high U(VI) adsorption properties of phosphoric acid-functionalized heteroatoms-doped carbon materials, Solid State Sci., 104 (2020) 106248, doi: 10.1016/j.solidstatesciences.2020.106248.
[5] L.X. Xie, Y. Zhong, R.J. Xiang, G.Y. Fu, Y.Z. Xu, Y.X. Cheng, Z. Liu, T. Wen, Y.Y. Zhao, X.Q. Liu, Sono-assisted preparation of Fe(II)-Al(III) layered double hydroxides and their application for removing uranium(VI), Chem. Eng. J., 328 (2017) 574–584.
[6] J. Jin, S.W. Li, X.Q. Peng, W. Liu, C.L. Zhang, Y. Yang, L.F. Han, Z.W. Du, K. Sun, X.K. Wang, HNO_3 modified biochars for uranium(VI) removal from aqueous solution, Bioresour. Technol., 256 (2018) 247–253.
[7] L.D. Troyer, F. Maillot, Z. Wang, Z. Wang, V.S. Mehta, D.E. Giammar, J.G. Catalano, Effect of phosphate on U(VI) sorption to montmorillonite: ternary complexation and precipitation barriers, Geochim. Cosmochim. Acta, 175 (2016) 86–99.
[8] Y.D. Zou, Y. Liu, X.X. Wang, G.D. Sheng, S.H. Wang, Y.J. Ai, Y.F. Ji, Y.H. Liu, T. Hayat, X.K. Wang, Glycerol-modified binary layered double hydroxide nanocomposites for uranium immobilization via extended X-ray absorption fine structure technique and density functional theory calculation, ACS Sustainable Chem. Eng., 5 (2017) 3583–3595.
[9] Z.S. Chen, S. Zhang, Y. Liu, N.S. Alharbi, S.O. Rabah, S.H. Wang, X.X. Wang, Synthesis and fabrication of g-C_3N_4-based materials and their application in elimination of pollutants, Sci. Total Environ., 731 (2020) 139054, doi: 10.1016/j.scitotenv.2020.139054.
[10] B.W. Hu, Q.Y. Hu, X. Li, H. Pan, X.P. Tang, C.G. Chen, C.C. Huang, Rapid and highly efficient removal of Eu(III) from aqueous solutions using graphene oxide, J. Mol. Liq., 229 (2017) 6–14.
[11] L.C. Tan, Q. Liu, X.Y. Jing, J.Y. Liu, D.L. Song, S.X. Hu, L.H. Liu, J. Wang, Removal of uranium(VI) ions from aqueous solution by magnetic cobalt ferrite/multiwalled carbon nanotubes composites, Chem. Eng. J., 273 (2015) 307–315.
[12] J.J. Liang, Z. Ding, H.M. Qin, J. Li, W. Wang, D.X. Luo, R.Y. Geng, P. Li, Q.H. Fan, Ultra-fast enrichment and reduction of As(V)/Se(VI) on three dimensional graphene oxide sheets-oxidized carbon nanotubes hydrogels, Environ. Pollut., 251 (2019) 945–951.
[13] H.Y. Ma, B.S. Hsiao, B. Chu, Ultrafine cellulose nanofibers as efficient adsorbents for removal of UO_2^{2+} in water, ACS Macro Lett., 1 (2012) 213–216.
[14] R. Hu, J. Xiao, T.H. Wang, G.C. Chen, L. Chen, X.Y. Tian, Engineering of phosphate-functionalized biochars with highly developed surface area and porosity for efficient and selective extraction of uranium, Chem. Eng. J., 379 (2020) 122388, doi: 10.1016/j.cej.2019.122388.
[15] W.-R. Cui, C.-R. Zhang, R.-P. Liang, J.-D. Qiu, Covalent organic framework hydrogels for synergistic seawater desalination and uranium extraction, J. Mater. Chem. A, 9 (2021) 25611–25620.
[16] S. Pai, M. Srinivas Kini, R. Selvaraj, A review on adsorptive removal of dyes from wastewater by hydroxyapatite nanocomposites, Environ. Sci. Pollut. Res., 28 (2021) 11835–11849.
[17] A. Szcześ, L. Hołysz, E. Chibowski, Synthesis of hydroxyapatite for biomedical applications, Adv. Colloid Interface Sci., 249 (2017) 321–330.
[18] R.-L. Ying, R.-X. Sun, Q.-q. Li, C.-n. Fu, K.-Z. Chen, Synthesis of ultralong hydroxyapatite micro/nanoribbons and their application as reinforcement in collagen scaffolds for bone regeneration, Ceram. Int., 45 (2019) 5914–5921.
[19] S.T. Wang, H.L. Liu, W. Liu, Q.Q. Zuo, Effect of low-molecular-weight organic acids on nano-hydroxyapatite adsorption of cadmium and lead, J. Biomater. Tissue Eng., 6 (2016) 433–439.
[20] M. Harja, G. Ciobanu, Studies on adsorption of oxytetracycline from aqueous solutions onto hydroxyapatite, Sci. Total Environ., 628–629 (2018) 36–43.
[21] R.F. Li, Y.Q. Liu, G.H. Lan, H.Y. Qiu, B. Xu, Q.X. Xu, N.Y. Sun, L.H. Zhang, Pb(II) adsorption characteristics of magnetic GO-hydroxyapatite and the contribution of GO to enhance its acid resistance, J. Environ. Chem. Eng., 9 (2021) 105310, doi: 10.1016/j.jece.2021.105310.
[22] R. Foroutan, S.J. Peighambardoust, A. Ahmadi, A. Akbari, S. Farjadfard, B. Ramavandi, Adsorption mercury, cobalt, and nickel with a reclaimable and magnetic composite of hydroxyapatite/Fe_3O_4/polydopamine, J. Environ. Chem. Eng., 9 (2021) 105709, doi: 10.1016/j.jece.2021.105709.
[23] E. Skwarek, A. Gładysz-Płaska, Y. Bolbukh, Adsorption of uranyl ions at the nano-hydroxyapatite and its modification, Nanoscale Res. Lett., 12 (2017) 278, doi: 10.1186/s11671-017-2042-8.
[24] W.T. Li, Q. Liu, R.R. Chen, J. Yu, H.S. Zhang, J.Y. Liu, R.M. Li, M.L. Zhang, P.L. Liu, J. Wang, Efficient removal of U(VI) from simulated seawater with hyperbranched polyethylenimine (HPEI) covalently modified SiO_2 coated magnetic microspheres, Inorg. Chem. Front., 5 (2018) 1321–1328.
[25] E. Broda, A. Gładysz-Płaska, E. Skwarek, V.V. Payentko, Structural properties and adsorption of uranyl ions on the nanocomposite hydroxyapatite/white clay, Appl. Nanosci., 12 (2022) 1101–1111.
[26] J. Liu, C.S. Zhao, Z.B. Zhang, J.L. Liao, Y.H. Liu, X.H. Cao, J.J. Yang, Y.Y. Yang, N. Liu, Fluorine effects on U(VI) sorption by hydroxyapatite, Chem. Eng. J., 288 (2016) 505–515.
[27] M.N. Han, L.J. Kong, X.L. Hu, D.Y. Chen, X.Y. Xiong, H.M. Zhang, M.H. Su, Z.H. Diao, Y. Ruan, Phase migration and transformation of uranium in mineralized immobilization by wasted bio-hydroxyapatite, J. Cleaner Prod., 197 (2018) 886–894.
[28] Y.H. Wu, D.Y. Chen, L.J. Kong, D.C.W. Tsang, M.H. Su, Rapid and effective removal of uranium(VI) from aqueous solution by facile synthesized hierarchical hollow hydroxyapatite microspheres, J. Hazard. Mater., 371 (2019) 397–405.
[29] H.H. El-Maghrabi, A.A. Younes, A.R. Salem, K. Rabie, E.-s. El-shereafy, Magnetically modified hydroxyapatite nanoparticles for the removal of uranium(VI): preparation,

characterization and adsorption optimization, J. Hazard. Mater., 378 (2019) 120703, doi: 10.1016/j.jhazmat.2019.05.096.
[30] T.H. Liu, Z. Xu, G.J. Duan, Y.P. Tan, Q.Q. Zhong, W.S. Wu, Adsorptive features of poly(acrylic acid-*co*-hydroxyapatite) composite for UO_2^{2+}, J. Radioanal. Nucl. Chem., 307 (2016) 1221–1230.
[31] G.J. Duan, H.N. Tian, H. Chen, R. Wu, Z. Xu, T.H. Liu, X.X. Peng, Amidoxime functionalized hydroxyapatite composites separate the uranium(VI) from aqueous solution, Desal. Water Treat., 225 (2021) 311–319.
[32] J.B. Yang, Q. Cao, Z.W. He, X.Y. Pu, T.T. Li, B.Y. Gao, X.H. Li, The poly(styrene-*co*-acrylonitrile) polymer assisted preparation of high-performance inverted perovskite solar cells with efficiency exceeding 22%, Nano Energy, 82 (2021) 105731, doi: 10.1016/j.nanoen.2020.105731.
[33] H.-J. Liu, P.-F. Jing, X.-Y. Liu, K.-J. Du, Y.-K. Sun, Synthesis of β-cyclodextrin functionalized silica gel and its application for adsorption of uranium(VI), J. Radioanal. Nucl. Chem., 310 (2016) 263–270.
[34] M. Manso, M. Langlet, C. Jiménez, J.M. Martínez-Duart, Hydroxyapatite coatings obtained by the thermal activation of polymeric sols, Int. J. Inorg. Mater., 3 (2001) 1153–1155.
[35] S. Zhang, X.W. Shu, Y. Zhou, L. Huang, D.B. Hu, Highly efficient removal of uranium(VI) from aqueous solutions using poly(acrylic acid)-functionalized microspheres, Chem. Eng. J., 253 (2014) 55–62.
[36] J. Liu, C.S. Zhao, G.Y. Yuan, Y. Dong, J.J. Yang, F.Z. Li, J.L. Liao, Y.Y. Yang, N. Liu, Adsorption of U(VI) on a chitosan/polyaniline composite in the presence of Ca/Mg-U(VI)-CO_3 complexes, Hydrometallurgy, 175 (2018) 300–311.
[37] S.I.Y. Salameh, F.I. Khalili, A.H. Al-Dujaili, Removal of U(VI) and Th(IV) from aqueous solutions by organically modified diatomaceous earth: evaluation of equilibrium, kinetic and thermodynamic data, Int. J. Miner. Process., 168 (2017) 9–18.
[38] A. Krestou, A. Xenidis, D. Panias, Mechanism of aqueous uranium(VI) uptake by hydroxyapatite, Miner. Eng., 17 (2004) 373–381.
[39] B.W. Hu, H.F. Wang, R.R. Liu, M.Q. Qiu, Highly efficient U(VI) capture by amidoxime/carbon nitride composites: evidence of EXAFS and modeling, Chemosphere, 274 (2021) 129743, doi: 10.1016/j.chemosphere.2021.129743.
[40] S.A. Sadeek, M.A. El-Sayed, M.M. Amine and M.O. Abd El-Magied, A chelating resin containing trihydroxybenzoic acid as the functional group: synthesis and adsorption behavior for Th(IV) and U(VI) ions, J. Radioanal. Nucl. Chem., 299 (2014) 1299–1306.
[41] C.H. Xiong, X.Z. Liu, C.P. Yao, Effect of pH on sorption for RE(III) and sorption behaviors of Sm(III) by D152 resin, J. Rare Earths, 26 (2008) 851–856.
[42] J. Li, J. Wang, W. Wang, X.T. Zhang, Symbiotic aerogel fibers made via in-situ gelation of aramid nanofibers with polyamidoxime for uranium extraction, Molecules, 24 (2019) 1821, doi: 10.3390/molecules24091821.